



THE GLOBAL SURFACE TEMPERATURE ANOMALY TIME SERIES AND ATTRIBUTION

Leonard J. Pietrafesa

Burroughs & Chapin Center P.O. Box 261954 Coastal Carolina University, Conway, South Carolina 29528 U.S.A.

Colin Gallagher

Department of Mathematical Sciences 0-110 Martin Hall Clemson University P.O. Box 34097 Clemson, South Carolina 29634 U.S.A.

ABSTRACT We study global surface temperatures from 1850 to 2016 via an empirical, mathematical methodology. Our study reveals internal modes of variability, periods of cooling and warming, both in the ocean and the atmosphere over land, ranging from seasonal to annual to inter-annual to multi-year to decadal to multi-decadal to centennial and overall warming trends. The oceanic rate of warming is less than two thirds of that of the atmosphere. By employing a mathematical methodology well known in ergonomics, this study causally links the upward rise in planetary surface temperature from the latter part of the 19th Century and into the 21st Century, to the contemporaneous upward rise in fossil fuel burning and suggests that if present fossil fuel burning is not curtailed there will be continued warming of the planet in the future.

KEYWORDS : .climate variability, climate change, fossil fuel burning, attribution.

1. Introduction

The Earth system absorbs the Sun's incoming short-wave radiation and radiates, stores or exchanges it at different rates via natural processes described by [1] and [2]. For a planetary condition of thermal equilibrium, the amount of total outgoing, long-wave radiation must equal the total amount of incoming, short-wave radiation. The fact that the outgoing radiation does not equal incoming radiation suggests that the planet's global body temperature varies both spatially and temporally. This is "climate variability". Of course the news media reports that 97% of scientists firmly believe that the climate has in fact been warming in the recent past, and refer to this as "climate change" or "climate warming". However there are also a reported 3% of U.S. scientists, along with some U.S. political representatives at federal and state levels who claim that no such global warming is occurring, or if it is, it is but a temporary aberration of a naturally occurring climate cycle that will be followed by a future cooling. On November 4, 2016, 193 nations signed on to the "Paris Climate Accord" and the Arc de Triomphe was brilliantly illuminated with the statement "Accord DeParis c'est fait" ("The Paris agreement is done") to celebrate the first day of the application of the Paris climate accord. <<https://www.nytimes.com/2017/05/31/climate/qa-the-paris-climate-accord.html>>. These nations took the step of agreeing to reduce carbon emissions globally.

A thorough discussion of the science surrounding global climate warming and cooling is presented by [3]. The authors point out that over periods of multiple decades the climate has been warming given the upward rise in temperatures reflected in the Global Surface Temperature Anomaly curve based on the best available global surface temperature data dating back to the middle of the 19th Century. Further they conclude this rise in global surface temperature may likely be attributed to human activity and land use. The authors also point out that natural phenomena such as changes in solar activity and Earth orbital adjustment could lead to global cooling over periods of hundreds to thousands of years and could result into a next ice age. In our study we focus on both oceanic and atmospheric surface temperature time series and dispel the more common belief that the atmosphere is controlling the overall surface temperature of the Earth. We also reveal relationships between the overall trends of the Earth's atmosphere and ocean temperatures, and fossil fuel burning. The global ocean covers 71% of the Earth's surface and contains 97% of the planet's water. The atmosphere blankets the entire planet. However, the heat capacity of the fluid phase of water is much different than that of either the fluid phase of air or ice; as relates to hydrogen bonding. The H₂O water molecule has a heat capacity and a latent heat of fusion 2nd only to that of NH₃, and this confers thermal stability to ocean waters, such that the heat capacity of the upper 3.5 meters of the global ocean is equivalent to that of the Earth's entire atmosphere. Land has a low thermal conductivity, so heat reservoirs on the land surface and in the atmosphere are very limited. Here, the planetary heat balance

components for the period from 1955 to 1998, based on the best observations at the time are presented in the pioneering work of [4]. Basically over that 44 year period, in units of 1022 Joules, these authors showed that of the total amount of incoming heat from the Sun: 14.5 was absorbed by the global ocean; 0.9 was absorbed by the continents; 0.8 was the heat required to melt continental glaciers; 0.7 was absorbed by the atmosphere; 0.3 was required to reduce the Antarctic sea-ice extent; 0.1 was needed to melt mountain glaciers; 0.005 was required to melt northern hemisphere sea-ice; and 0.002 was required to melt perennal Arctic sea-ice. Thus these authors estimated that the ocean absorbs approximately 21 times as much as does the atmosphere. Thus, the global ocean absorbs ~ 85% of the Sun's incoming radiation.

Given the several thousands of meters of oceanic depths, and the heat capacity of water, enormous quantities of heat are stored in the global ocean for long periods of time, with some of the stored heat released to the atmosphere. When the ocean releases heat and moisture into the atmosphere climate factors and conditions are altered and atmospheric eddies, aka "atmospheric storms", form. Heat is then redistributed by the atmosphere, principally from the Equatorial zone to the Polar zones. Likewise oceanic "western boundary currents" (WBC's), such as the Gulf Stream, the Kuroshio, the Brazil, the Agulhas, and the East Australia, move heat from Equatorial to Polar Regions and large scale vertical plane ocean circulations such as the southward flowing deep branch of the Atlantic Meridional Overturning Circulation (the MOC) which moves cold, saline water from the Poles towards the Equator, thus having the net effect of increasing the meridional heat distribution in a poleward direction. The MOC [5] has been referred to as the Thermohaline Circulation (THC) of the ocean, that is the part of the circulation controlled by temperature and salinity variations, but the two are synonymous wherein the MOC is the zonal integral of the meridional velocity while the THC is a mechanism involved in the overturning. This begs the question: What does the overall heat content record actually mean in terms of any associated increases or drops in the surface temperature of the global ocean. In Figure 1, 3-month and 12-month averaging is done to depict the seasonal and annual curves. In our study we will not do any block or moving averaging of the data. Rather we will employ a mathematical methodology that can decompose non-stationary and non-linear time series of data into temporal views of the data that we can work with mathematically.

In Figure 1, we present seasonal and yearly anomaly data from the averages of global oceanic heat content data collected from the ocean surface down to 700 m over the period 1955-2010 using data obtained variously from the U.S. Navy, academic institutions, other countries and more recently, the National Oceanic and Atmospheric Administration (NOAA). The data were obtained from the NOAA National Ocean Data Center and processed and analyzed in [4] and [6]. Heat content is variable on seasonal and annual bases and rose from the

relative heat anomaly of -5×10^{22} Joules to $+13 \times 10^{22}$ Joules (J), an increase of 1.8×10^{22} J (Figure 1). What is responsible for this rise in heat in the global ocean? Is incoming heat from the Sun responsible for the rise in heat content over the 56 year period? How does the oceanic heat reservoir redistribute its heat internally and externally? We address these questions below. It is of note here that the time series displayed in Figure 1 appear to be highly non-stationary and non-linear. This is known to be true of global surface temperature data as well, as we will present and discuss below.

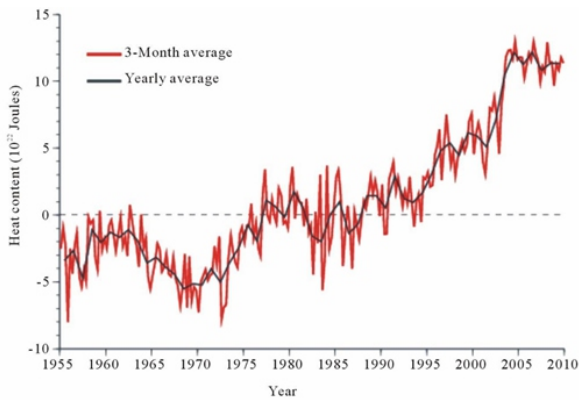


Figure 1. The 3-month average (red line) and annual average (blue line) of the global ocean heat content anomaly from the surface down to 700 m depth, 1955 through 2010. Reproduced with permission of Dr. S. Levitas (p.c.).

Recently, oceanic heat content studies from 1950 – 2015 have been reported upon in [7] and [8], and both include the global oceanic data derived from the Argo float constellation that the U.S. and other nations established in 2000 and have steadily increased thereafter. Presently Argo has become a global array of 3,800 free-drifting profiling floats that measure the temperature and salinity of the upper 2000 meters of the global ocean, across all ocean basins. The ARGO program has allowed continuous spatial and temporal monitoring of the temperature, salinity, and velocity of the ocean, with all data being relayed and made publicly available within hours after collection. The authors concur that up until about 1980 there was a gradual increase of heat content with significant increases thereafter; as suggested in Figure 1. Moreover, the studies found that the five ocean basins are sequestering heat at different rates down to 2000m with the Atlantic Basin having had the largest percentage increase with its rate of heat content being 3.5 times that of the Pacific Ocean Basin. The causes are not yet known.

In the study reported on below, we will extend beyond the temperatures of just the global surface atmosphere above land to temperatures of the surface of the global ocean as well. It could be argued that while much attention was paid to the global surface atmospheric temperature record, and rightfully so as greenhouse gases have built up in the atmosphere, not enough attention has been paid to the global ocean temperature record in-kind. We will investigate the variability of oceanic surface and atmospheric land surface temperatures and oceanic heat as documented in global time series records. We will investigate the variability of temperature and heat as documented in several well-known time series records and see if we can shed new insights into what these records reveal regarding the Earth's Climate system. As alluded to above, we expect that the Earth's surface temperatures, which define our climate system, are created by and characterized by non-linear and non-stationary processes, so we will utilize an empirical, mathematical data adaptive technique which can deal directly with these types of data, to decompose the data. The Empirical Mode Decomposition mathematical methodology was first introduced and detailed in [9] and shown to be able deal with both non-linear and non-stationary time series; as opposed to more conventional mathematical methodologies, which cannot do so.

1. Empirical Mathematical Decomposition Analytics

Empirical Mode Decomposition (EMD) and its offspring the Ensemble EMD (or EEMD) is a two stage adaptive and temporally local time-frequency data decomposition mathematical method.

Basically, the “ensemble” method adds white noise to the signals and involves multiple decompositions of the signals; all described below. It is noted that the detailed description of the EMD and EEMD methods can be found in a series of key papers, including [9], [10], [11], [12], [13], [14] and [15]. In the EMD, the Hilbert Transform, HT, [9] is employed. After a time series is decomposed into IMFs, natural amplitude-frequency modulated oscillatory functions, various methods can be applied to obtain instantaneous frequencies for each IMF that lead to time-frequency-energy representation of data. The challenge of frequency modulation in signals was first discussed some seven decades ago in both [15] and [16]. More recently, a new methodology [17] was applied to calculate the accompanying imaginary part of an IMF and to obtain the complex expression of an IMF from which the instantaneous amplitude and frequency can be calculated as originally addressed in [9] and [10]. Thus, via the employment of the HT, a continuous time series of data $x(t)$ is decomposed in terms of “intrinsic mode functions” (IMFs), c_j , i.e.,

$$x(t) = \sum_{j=1}^n c_j(t) + r_n(t) \quad (1a); \text{ where } c_j(t) = a_j(t) \cos \left[\int \omega_j(t) dt \right] \quad (1b),$$

where r_n is the residual of the data $x(t)$, after n intrinsic mode functions (IMFs) are extracted from the instantaneous frequency, ω , from high frequency to low frequency. Intrinsic modes or IMFs, from $j=1$ to the finite number “ $j = n$ ”, are determined via a “sifting” process and which constitute the limits of the integral (i.e. 1 to finite number “ $j = n$ ”). We note that “instantaneous frequency” is defined in context and can be considered as the local mean for IMF c_n . Clearly, The IMFs expressed in Equation (1b) are simple oscillatory functions with relatively slowly varying and non-negative amplitude and relatively fast changing and non-negative frequency at any temporal location. In practice, the EMD is implemented through a sifting process that uses only local extrema. From any data set, $x(t) = r_{j-1}$, say, the procedure that we will employ below is as follows: 1) identify all the local extrema (the combination of both maxima and minima) and connect all these local maxima (minima) with a cubic spline as the upper (lower) envelope; 2) obtain the first component h by taking the difference between the data and the local mean of the two envelopes; and 3) treat h as the data and repeat steps 1 and 2 as many times as is required until the envelopes are symmetric about zero within a small tolerance. The final h is designated as c_j . A complete sifting process stops when the residue, r_n , becomes a monotonic function or a function only containing one internal extreme from which no more IMF can be extracted. To recover the original time series, one simply picks a time along the x axis and sums the values of the IMF modes at that same time throughout. The original data point will be the result of the addition.

The impetus for the EEMD was that EMD was seen to have an IMF “mode mixing” problem, defined as any IMF consisting of cross-talk between oscillations of neighboring IMFs. Since real data generally contain a certain amount of random noise or intermittences, an important issue became apparent, basically whether the decomposition was sensitive to unknown noise; because the decomposition was solely based on the distribution of extremes; which occasionally lead to a difficulty in the physical interpretation of IMFs. However, to solve this problem, the “Ensemble” - EMD (EEMD) was developed [12] and [17]. In this advance, and somewhat counter-intuitively, multiple noise realizations were added to one time series of observations to mimic a scenario of multiple realizations from which an ensemble average approach for corresponding IMFs could be used to extract scale-consistent signals. The major steps of the EEMD method are: 1) add a white noise series to the targeted data; 2) decompose the data with added white noise into IMFs; 3) repeat Step 1 and Step 2 nominally 100 times, but with different white noise series each time; and 4) obtain the (ensemble) means of corresponding IMFs of the decompositions as the final result. The effects of the decomposition using the EEMD are that the added white noise series cancel each other, and the mean IMFs stay within the natural dyadic filter windows; as discussed in [12] and then [17] and [18]. This was found to eliminate mode mixing, to preserve the dyadic property of EMD, and to lead to stable IMF decompositions. Therefore, this advance has rendered the EMD/EEMD method to be very robust.

Before proceeding with our EEMD decompositions, we need to visit the definition of and the methodology of computing a “trend”. If you visually interrogate the three water level time series presented in Figure 3, there is a very strong sense of both N-S and N-L temporal

variations. As such, it is not clear that any conventional simple averaging process can be utilized to reflect what information is buried in the multiple time series. This underscores the importance of clearly defining what is meant by trend. The definition of a trend proposed in [19] is: “the general drift, tendency or bent of a set of data”. In [20], the definition of a “trend” is “a long term change in the mean”. But a difficulty with this latter definition is determining what is meant by “long term”. What if there were variations in climatic variables that exhibit a 50 year cycle. If one were to have only 20 years of data, then the 50 year cycle would appear to be a trend. But if there were 120 years of data then the 50 cycle would go through 2.5 cycles and thus be evident. So in speaking of a “Chatfield trend” (in [20]), we must take into account the number and span of observations available and then make a subjective assessment as to what constitutes “long term”. In [21], the definition alludes to “a trend in mean as comprising all frequency components whose wavelength exceeds the length of the observed time series”. However, for N-L, N-S datasets, none of these definitions ([19], [20] or [21]) are mathematically tractable. How can you mathematically compute something that you cannot mathematically define? In 2007, a publication appeared in the peer reviewed literature which changed this confusing situation.

In our opinion the seminal publication of [22] put forward a logical definition of “a trend” which is appropriate for any N-S and N-L time series. The authors said: “a trend is an intrinsically determined function within the temporal span of the data, and a function in which there can be at most one extremum within that temporal span of data”. Being intrinsic, the method that should be employed to derive a trend has to be adaptive that is, it must suit the time span of the data. Thus the definition of trend in [22] does make a presumption of the existence of a time scale, related to the span of the data; a logical, mathematically based definition. All the above requirements suggested the EMD method as the logical choice for an algorithm that could determine the trend in any continuous data set. The ‘gravest’ intrinsic mode or rather the lengthiest mode of a time series that can be determined by employing the EMD methodology, one which can go up or down, or down and or up, in amplitude, so that there is only one respective maximum or only one respective minimum in this mode, then defines the “trend” of the time series. Once the trend of a time series is determined via the EMD, the corresponding de-trending operation can be implemented. With this definition of trend, the variability of the data over inherent, intrinsic time scales can next be derived. We will employ the advanced form of EMD, the Ensemble EMD (EEMD), as described above, to decompose the data set time series that we will study, and identify all intrinsic modes present in each, including the trend.

In Figure 2 we see the EEMD of the Global Heat Content 3-monthly averaged time series over the 57 year period of 1955-2010. The decomposition reveals 7 intrinsic modes. IMFs are: C1, 3 - 6 monthly with an “absolute amplitude” (AA) of $4(10^{23})$ J; C2 annual to inter-annual and AA $2(10^{23})$ J; C3 a 3 - 4 year cycle, with AA $1.5(10^{23})$ J; C4 a 10-12 year cycle, with AA $1(10^{23})$ J; C5, a 21-22 year cycle, and AA $2(10^{23})$ J; C6, a 32 -35 year cycle, and AA $(0.7) (10^{23})$ J; the gravest mode (red line, upper panel), a trend which has risen over the 57 year record, from $-3.5(10^{23})$ J to $+11(10^{23})$ J, or $1.45(10^{23})$ J.

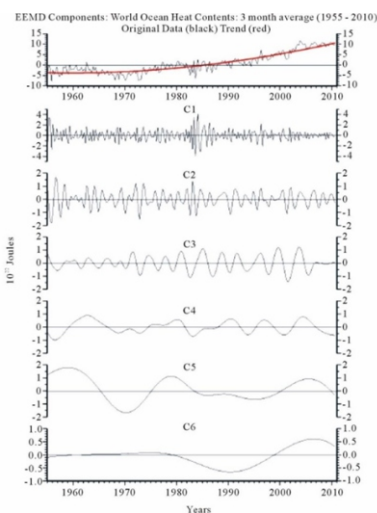


Figure 2. EEMD of the 3 month average global ocean heat content time series from the surface of the ocean down to 700m. There are 7 IMFs, with C7, the Trend, showing a significant rise.

In Figure 3 we present the monthly averaged Sunspot Solar activity over the 162 year period from 1849 through 2009. In the 161 year record there are 9 IMF modes, including: a relatively flat trend, the red line; Mode 8, a long period, multi-decadal cycle of ~155 years with AA of 20 events; Mode 7, 55 - 60 years and an AA of 30 events; Mode 6, 22 years and AA of 30 events; Mode 5, 10-12 years, with AA of 80 events; and Modes C1, monthly, C2, 3-6 months, C3, annual, and C4, 2-3 years, all displaying bursts of activity centered about 11 years, with AA of 30 events for C3 and C4, and 40 for C1 and C2. The overall trend (red line, upper panel in Figure 3) ranges from 50 to 51.5 events over the 161 year period of record. Thus, Oceanic Heat Content down to 700 m is in sync with Solar activity for IMFs of 3 months, annual, 3-4 years, 10-12 years, and 22 years. While the Sunspot trend is essentially flat over 167 years, the Heat Content has risen significantly over 57 years.

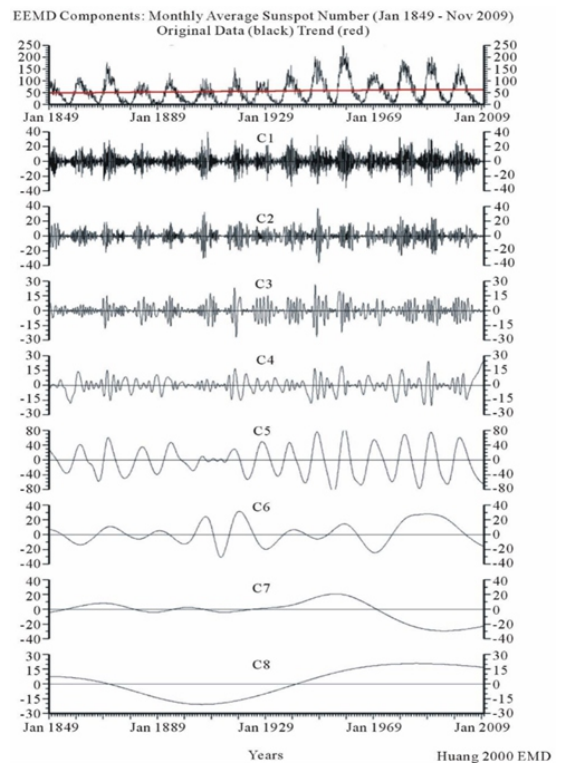


Figure 3. Monthly Sunspot activity from 1849 -2010. There are nine IMFs and the overall trend is basically flat.

2. Global Ocean and Land Based Atmospheric Temperature Anomaly Time Series

In Figures 4, 5 and 6 below, we present the basic monthly averaged time series and EEMD IMF decompositions, of Global Surface Temperature Anomaly data from 1850 through 2016 for the: Figure 4, the land-based atmosphere (the GLSTA); Figure 5, the global sea surface (the GSSTA); and Figure 6, the combined land-based atmospheric surface and the ocean surface (or the GLSTA + the GSSTA, the GSTA). These three time series are continuously compiled jointly by the Climatic Research Unit and the UK Meteorology Office, Hadley Centre: <http://www.cru.uea.ac.uk/cru/info/>. The credibility of the data are without question and are revered by the global scientific and technology communities. We note that the 167 year time series all display 10 IMF modes with the 10th in each case being the overall trends of the land-based atmosphere, the ocean surface and the combination of the two. The units of the vertical axes are +/- °C.

The IMF modes of the GSSTA and GSSTA are essentially the same for the ocean surface and for the atmosphere over land, save for differing AAs. Modes 1 are bi-monthly to seasonal, Modes 2 are 6-monthly, Modes 3 are annual, Modes 4 are 2-3 years, Modes 5 are 4-6 years,

Modes 6 are 10-12 years, Modes 7 are 20-22 years, Modes 8 are 60-70 years, Modes 9 are 105 years and Modes 10 are the overall trends. The trend of the GLSTA Ranges from -0.4340 OC in 1850 to +0.7780°C in 2016 for a total rise of +1.2120 °C. The GSSTA ranges from -0.3297 OC in 1850 to +0.4486 °C in 2016 for a total rise of + 0.7783 oC. The GSTA or combined ocean surface and land surface rises in temperature have gone from -0.3699 in 1850 to +0.5501 °C in 2016 for a total rise of +0.9200°C. As such the ocean surface temperature, as represented via the GSSTA, has risen at a much slower relative rate as has that of that of the atmosphere over land, the GLSTA. The GLSTA rate of warming from 1850 through 2016 is 7.257485 (10-2) °C/decade. The GSSTA rate of warming from 1850 through 2016 is 4.66048 (10-2) °C/decade. The combined GSTA is 5.550898 (10-2)°C/decade.

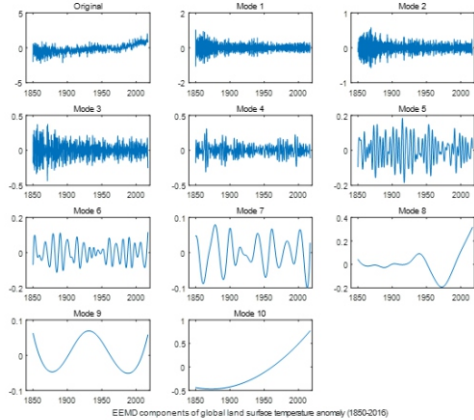


Figure 4. The EEMD decomposition of the GLSTA revealing 10 modes. Upper left panel is the original time series. IMF 10 is the overall time series trend.

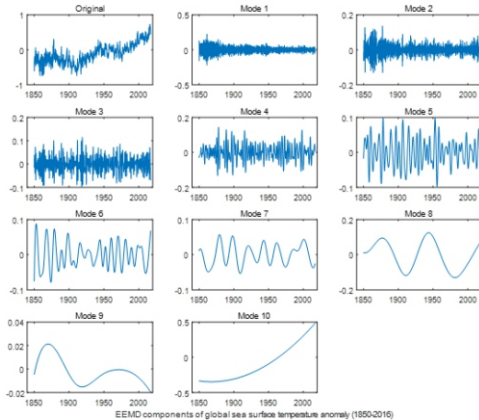


Figure 5. The EEMD decomposition of the GSSTA revealing 10 modes. Upper left panel is the original time series. IMF 10 is the overall time series trend.

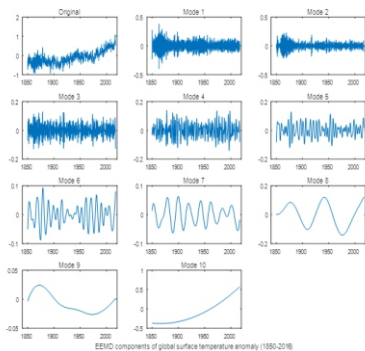


Figure 6. The EEMD decomposition of the GSTA revealing 10 modes. Upper left panel is the original time series. IMF 10 is the overall time series trend.

We note in Figure 4, that for the GLSTA, the relatively low frequency modes of IMFs 3 and 4 have AAs of 0.4 oC, IMF 5 has an AA of 0.2 oC and IMFs 6 and 7 have AAs of 0.1 oC. IMF 8's amplitude ranges from -0.2 to +0.35 oC, which is relatively considerable. The similar temperature IMFs are present in the GSSTA IMF decomposition shown in Figure 5 and for the combined temperature anomaly time series, the GSTA, in Figure 6. All IMF modes contribute in amplitude in a nominally equitable manner. What this implies is that high to low frequency variability contributes to a monthly averaged surface temperature significantly at any particular time. One cannot ignore where the planet is in its journey of its natural, intrinsic, internal surface temperature variability. Thus periods of relative warming and or cooling occur naturally by the additive and or subtractive disposition of the natural variability of the physically based natural modes of variability in surface temperatures; all riding atop overall land, ocean and combined trends. These modes of variability are summarized in Table 1. The Trend end points for the GLSTA, GSSTA and GSTA are presented in Table 2.

Table 1. IMFs of surface temperatures shown in Figures 4, 5, 6 (in units of Years).

IMF #	1	2	3	4	5	6	7	8	9	10
GLSTA	0.25	0.5	1	2-3	4-6	10-12	20-22	60-70	105	167
GSSTA	0.25	0.5	1	2-3	4-6	10-12	20-22	60-70	105	167
GSTA	0.25	0.5	1	2-3	4-6	10-12	20-22	60-70	105	167

Table 2. Trends of GSTA, GLSTA and GSSTA as is (Figures 4, 5, 6) and Normalized to Zero Onset.

Year	GSTA (°C)	GLSTA(°C)	GSSTA (°C)	GSTA(°C)	GLSTA(°C)	GSSTA(°C)
1850	-0.3699	-0.4340	-0.3297	0.0	0.0	0.0
2016	0.5501	0.7780	0.4486	0.9200	1.2212	0.7883

In Figure 7, we see in the upper left panel, that from 1850 to 1895 the air temperature over land actually decreased slightly (blue line), so there was a global cooling over land globally that persisted for about 45 years. Then in 1895 the air temperature over land around the entire planet reached its prior value in 1850 and then continued to rise positively up through 2016. The same scenario was true for the surface waters of the global ocean, (red line), but with a lesser degree of cooling crossing from relative cooling to overall warming about 1880. The combined atmosphere and ocean time series (black line), follows closely that of the ocean and also moved from cooling to warming about 1880. The air over land is relatively cooler than that of the surface of the ocean until about 1915 when the lines cross and air temperatures on land rose at a more rapid rate then did those of the ocean. The three trend curves, all normalized to zero onset, are overlaid in Figure 7. The air over land and ocean surface trend curves diverged significantly up through 2016. Table 2 presents the end points for the three Mode 10 trends and the zero normalized, adjusted end points. The global oceanic surface warming rate is shown in Figure 7 to be 64.2% of that of the atmosphere over land or alternatively the surface warming over land is 155.7% greater than that of the warming of the surface of the global ocean.

If one were to estimate global warming by only the increase of temperatures over land one would obviously overestimate the true overall planetary warming. By the same token, using the rise of the temperature of surface waters of the global would underestimate the total global rise. Obviously the ocean is a buffer against global heating but is significant also. In [23], the famous 2007 IPCC Nobel Prize winning report, straight lines were drawn through the entire temperature anomaly time series, the GSTA, to estimate the rate of rise, or slopes of the temperature curves, of global temperatures. The IPCC straight line slope estimates were 0.045OC/decade over the full GSTA temperature record, 0.074 OC/decade over the prior 100 years, 0.128 OC/decade over the previous 50 years and 0.177 OC/decade over the latter 25 years of the record. From the straight lines, the different rates of rise of temperatures can be estimated. If we were to do a similar straight line estimate, ours would be 0.073oC/decade for the GLSTA, 0.047oC/decade for the GSSTA and 0.055oC/decade for the GSTA. However, the Trend curves shown in Figure 7 display periods of

cooling over the first parts of the time series. Clearly straight lines are not the physically plausible manner in which trends of non-linear time series can be estimated. Only the EEMD method can do so, as explained above. We also provide the derivatives of the Trends, i.e., the slopes or time rates change of the Trends or Modes 10, in Figure 8.

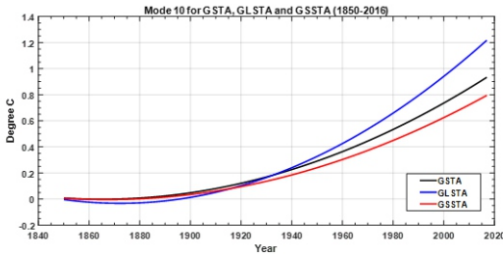


Figure 7. The overall time series length trends of the GLSTA, the GSSTA and the combined GSTA.

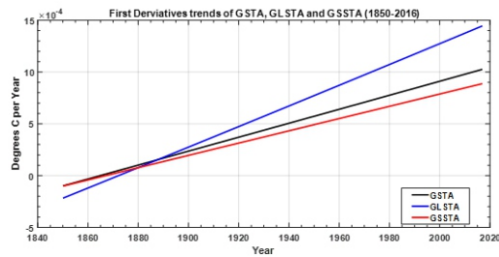


Figure 8. The time rate of change, or slopes, of the Trends of the surface temperatures of the planet or of the air over global land, the GLSTA (blue), of the surface of the global ocean, the GSSTA (red), and the combined time series, the GSTA (black) from 1851 through 2015 (as the two end points are lost in the calculation of the slopes or first derivatives, of the lines).

In Figure 8 we see the yearly time rates of change or slopes of the Trend time series presented in Figure 7. At the onset of the time series in 1850, all three surface temperature anomaly Trend curves are negative, indicating an initial cooling trend of the air over land and of the ocean's surface as well. The time rate of the cooling of air over land was greater than the time rate of cooling of the ocean surface during this early portion of the temperature time series. In 1880 the temporal rate of warming of air over land exceeded that of the ocean surface which has continued to be the case through 2016. The trends in warming have obviously occurred at ever increasing rates. The air over land cools more rapidly and also heats more rapidly than do the ocean surface waters. The rates of warming of air and ocean surface have increased in a positive manner since the onset of the time series. The highest rates of warming occurred between 2015 and 2016. We next turn to the Fossil Fuel Burning time series dating back to 1751.

3. Fossil Fuel Burning, Carbon Emissions and Co₂

The Fossil Fuel Burning, i.e. the Carbon Emissions (CE) time series, beginning in 1751, is provided to us via Global CO₂ Emissions from Fossil-Fuel Burning, Cement Manufacture, and Gas Flaring: 1751-2013. Confirming sources include [24] and [25]. All emission values are expressed in "million metric tons" of carbon (106 MTs or MMTs). To convert these values of carbon into units of carbon dioxide (CO₂), multiply the fossil fuel burning values by 3.667. (http://cdiac.ornl.gov/trends/emis/tre_glob.html). In Figure 9, the 263 year time series of CE, from 1751 through 2103, is presented. Year 2013 is the last year for which CE data is available to external users. Clearly from 1751 up until about 1850 not much CO₂ production was occurring globally having ranged from 3 MMTs in 1751 to 54 MMTs in 1850. As shown in Figure 9, in the latter half of the 19th Century carbon emissions increased considerably; with a slight decrease during World War II, followed by a dramatic upsurge around 1949 up to 2013 values; with occasional increases or decreases on an annual basis in the overall CE time series. The temporal, annual rate of change of CE was essentially flat from 1751 through the mid latter half of the 19th Century when the annual rate of carbon burning began to be spiky (Figure 9). Reasons for that undoubtedly are related to the advances in the industrialization of different parts of Europe and the emergence of industry in the U.S. In Figure 10, we present the EEMD of the 263 year

CE time series by year and in MMTs of carbon emissions.

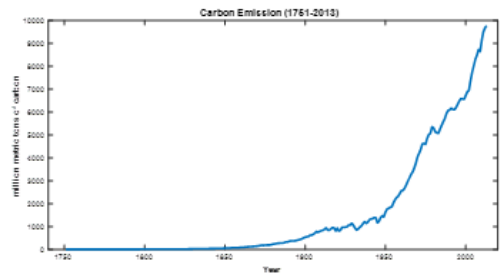


Figure 9. The Carbon Emissions (CE) or Fossil Fuel Burning Time series from 1751 through 2013.

In Figure 10, we see that the 263 CE year time series, contains 8 internal modes; IMF 1) annual with maximum AAs of 250 MMTs; 2) 3-5 years with maximum AAs of 250 MMTs; 3) 12- 15 years with maximum absolute AAs of 250 MMTs; 4) 23-25 years with maximum AAs of 500 MMTs; 5) 85-95 years with maximum AAs of 500 MMTs; 6) about 135 years and maximum AAs of 1600 MMTs; 7) about 260 years and maximum AAs of 50 MTs; and 8) the overall 262 year trend from 3 MMTs in 1753 to 54 MMTs in 1850 to nearly 104 MMTs in 2013. In Table 3, we present the end points of the curves presented in Figures 9 and 10.

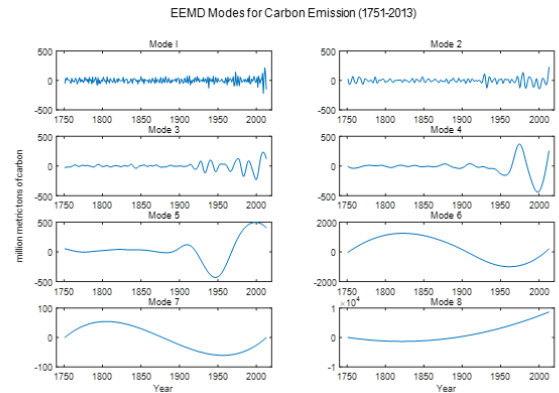


Figure 10. The EEMD of the CE times series. There are 8 IMFs. IMF 8 is the overall trend.

Table 4. The end points of the curves presented in Figures 9 and 10.

Year	GSTA (°C)	GLSTA(°C)	GSSTA (°C)	Carbon Emissions MMTs or MTs X 106
1751	N/A	N/A	N/A	3
1850	-0.3699	-0.4340	-0.3297	54
2013	0.5137	0.7265	0.4160	9776
2016	0.5501	0.7780	0.4486	N/A

In Figure 11, the GSTA, GLSTA and GSSTA overall trends are plotted versus the CE raw data. The three surface temperature time series begin in 1850 while the carbon emissions curve dates back to 1751. To normalize the comparison of the Trends, we created plots of only "trends" of the time series shown in Figure 11 (but not shown). To create the CE trends the apparent "bumps" created by IMFs 1 – 7 of the CE time series have been subtracted out and all that remains is the Overall Trend of the CE data time series. The visual similarities in the Trend Curves of the Surface Temperature Data and the Fossil Fuel Burning are striking but not shown as the point is made by Figure 11 that GSTA and CE curves essentially overlay. However we understand that visual correlation does not convey causality. In Table 4, we present the IMFs of the GLSTA, GSSTA, GSTA and CE curves. The CE IMFs are based on annual data whereas the temperature anomaly data are monthly, and therefore the CE IMF modes are all => than annual. In Figure 12a we present the annualized time rate of change of the raw fossil fuel CE curve (Figure 9) and in Figure 12b, we present the annualized time rate of change of the CE Trend (Mode 8).

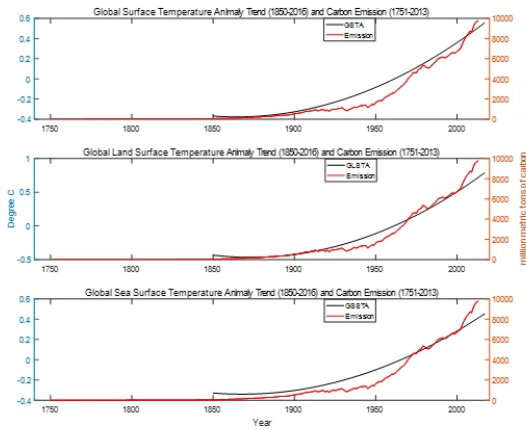


Figure 11. The CE Annual Time Series from 1751 – 2013 versus: Upper Panel, the 1850-2016 GSTA Trend; Middle Panel, the 1850-2016 GLSTA Trend; and Lower Panel, the 1850 – 2016 GSSTA Trend.

Table 4. IMF#s of surface temperatures shown in Figures 4, 5, 6 and CE's (in units of Years).

IMF#s (in Yrs)	1	2	3	4	5	6	7	8	9	10
GLSTA	0.25	0.5	1	2-3	4-6	10-12	20-22	60-70	115	167
GSSTA	0.25	0.5	1	2-3	4-6	10-12	20-22	60-70	115	167
GSTA	0.25	0.5	1	2-3	4-6	10-12	20-22	60-70	115	167
CE- MMTs	1	3-5	12- 15	23- 25	85-95	135	260	262		

At this point in the discussion we have shown visual correlations between the trends in global surface temperatures and fossil fuel burning but not causality. One could proceed here with Cross-Correlations of the Surface Temperature time series and the Carbon Burning trends as suggested in Figure 11. However we point out that if a family had a new human baby on Day 1, and the same family's dog gave birth to puppies on Day 1, that by Day 1091, three full years later, if both the human child and the puppies were properly nourished, they all would have gained weight and grown in length, relative to their species. However their upward trends while visually correlated, would not be causally correlated; and therefore there is no attribution between the GSTA and the CE. We will now explore the latter possibility.

4. Cross-Correlations of Planetary Surface Temperatures and Fossil Fuel Burning

Next, we will attempt to relate the time series of the GLSTA and the GSSTA to the CE. As the CE time series is annual, so we must create annual time series of the surface temperature time series. Further, since the CE annual time series dates back to 1751 but the temperature time series date back to 1850, the CE time series must be cut to 1850 to be consistent with the temperature time series. Finally, it is of note that in our initial cross correlation calculations of CE and surface temperatures from 1850 through 2013, we find very strong relationships between the CE curve to the GSSTA, GLSTA and GSTA trend curves. However as the time series values of temperatures, which began in 1850, could be criticized as being globally problematic, we only consider the more recent time series of global surface temperatures, and we choose time series commencing in 1950, when global values, which following WWII became routine, and are thus without question, regarding validation. We also will only utilize raw time series with no EEMD having been performed.

We note up front that proving absolute causality between surface temperatures and fossil fuel burning without running a global climate model that contains all sources and sinks of heat which could affect global surface temperature is a challenge. We also note that causality is the agency or efficacy that connects one process (the cause) with another process or state (the effect), where the first is understood to be partly responsible for the second, and the second is dependent on the first. In general, a process has many causes, which are said to be causal

factors for it, and all lie in its past. However, here we can consider causality in the Granger Causal Relationship sense [26]. This approach has been used in studies in the field of “econometrics” theory and applications to great success.

In [26] the idea was presented that if series {xt} contributes causally to series {yt}, then past values of {xt} should improve predictions of series {yt}. This type of causality is established by first modeling {yt} in terms of the past values of {yt} through an autoregressive (AR) process, then adding past values of series {xt} to create a second model. If the second model is statistically better than the first, then we have established causality in the Granger sense, the Granger Causal Relationship (GCR). We will fit all of our models using Gaussian maximum likelihood estimators and our hypothesis tests will be based on the asymptotic normality of the parameter estimates and we will make use of the estimated standard errors based on “optimized likelihood” presented in [27]. All of our statistical analysis is performed using the R software and the codes are available from the authors.

We first consider establishing a causal relationship between the carbon burning time series, the CE, ({x_t}) and the global sea surface temperature time series, the GSSTA ({y_t}) in the latter half of the 20th century. Our first model relates GSSTA to past values of GSSTA. Using Akaike's Information Criterion (AIC; in [28]) we select the order of the auto-regression to be 3; that is that each year's GSSTA is related to the values from the last 3 years. We use the Box-Ljung “goodness of fit” test, presented in [29] to verify that the AR model adequately models the autocorrelation (up to lag 20) in the GSSTA series; the p-value of 0.1471 indicates that there is no significant autocorrelation left in the residuals from the fitted model:

(2)

$$(2) \quad y_t = 0.113 + 0.7534y_{t-1} - 0.2654y_{t-2} + 0.4350y_{t-3} + e_t$$

From Figure 12a we can see that there appears to be a strong linear relationship between the sea surface temperature anomaly in year t and the carbon burning in year t-1. To establish the GCR, we now add the previous year CE value to the model. The resulting model is given by (3):

(3)

$$(3) \quad y_t = -0.57 + 0.6585y_{t-1} - 0.2798y_{t-2} + 0.3509y_{t-3} + 0.0066x_{t-1} + e_t$$

We can test for statistical significance of each fitted coefficient using the asymptotic normality of the Gaussian maximum likelihood estimators [27]. We conclude with a p-value of 0.0009, that the coefficient of xt-1 is non-zero. In other words, the predictive model for GSSTA is statistically better if the previous year of CE is included. We have thus established causality in the Granger sense.

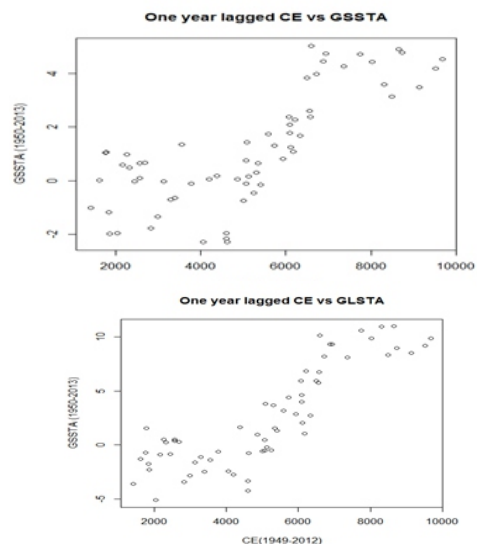


Figure 12. a) left, the GSSTA vs. the CE, with a 1-year Lag; b) right, the GLSTA vs. the CE with a 1-year Lag.

We note that in this analysis we selected the data beginning in 1950 and there is no question concerning the quality of the global data. However, we find that a similar analysis can be conducted starting at any point in the past. The same analyses beginning each decade in the first half of the 20th Century, i.e., in years 1900, 1910, 1920, 1930, 1940, and 1950, resulted respectively in p-values of 0.00005, 0.0002, 0.00002, 0.0002, 0.003, 0.009, for the coefficient of $xt-1$. In each case we conclude the model using the previous year CE is statistically better than the AR(3) model alone; and the CE series significantly improves predictions for GSSTA over the model based solely on past GSSTA values. Regardless of starting time point in the 20th century one finds statistical evidence of a causal relationship between CE and GSSTA.

Alternatively, one could attempt to establish that the GSSTA series "causes" the variability in the CE time series in the same manner as above. However, the result is that the lagged value of GSSTA does not provide statistically significant improvement in predicting the CE. For example, for the data starting in 1950 a fourth order autoregressive model fit to $\{xt\}$ which also uses the previous year GSSTA ($yt-1$), results in a test for significance of the coefficient for GSSTA with a p-value of 0.65. We would then not conclude that GSSTA is causing outcomes for CE.

In Figure 12b, we present the results of the the GLSTA vs the CE. Figure 12b consists of a plot of the GLSTA series on the vertical axis with corresponding points from the CE series in the previous year. We again see visual evidence of correlation, which indicates the previous year CE may improve prediction of the values of the GLSTA series. As with the GSSTA series, we investigate Granger causality. We again use AIC to select an optimal order of auto-regression and use the Ljung-Box test to verify that we have adequately model the autocorrelation in GLSTA. The fitted model predictive model uses past values of GLSTA and the previous year CE to predict each year's value of GLSTA $\{yt\}$, is given by (4) and presented in Figure 15: $(4) y_t = -5.5 + 0.3527y_{t-1} + 0.3543y_{t-2} + 0.0016x_{t-1} + e_t$. We next test to determine if the coefficient for $xt-1$ is statistically non-zero and find a p-value of 0.00000009, which indicates that CE provides statistically significant improvement in predicting GLSTA after accounting for the information in the past values of GLSTA. We have again established GCR. As is the case with the GSSTA series, the statistical analysis results in the same causality conclusion regardless of the starting decade in the 20th century.

Proceeding in a similar manner we find a predictive model for the GSTA $\{yt\}$ based on past values of the GSTA and the previous year CE $\{xt\}$, as given by (5), (and not plotted as the plots are alike those in Figures 12a and 12b): $(5) y_t = -7.30 + 0.4344y_{t-1} + 0.32 \{0.3y_{t-2}\} + 0.0022x_{t-1} + e_t$. Once again the number of lagged values of GSSTA are selected via AIC and the Ljung-Box goodness of fit test indicates that the autoregressive structure successfully models the autocorrelation in $\{yt\}$. The estimated coefficient for $xt-1$ of 0.0022 has an estimated standard error of 0.005, which results in a p-value of 0.00001 indicating that the previous year CE is highly correlated with GSSTA. We again conclude GCR.

Discussion and Conclusions

Since the latter part of the 19th Century up to the present, the reported overall rise in global surface temperatures has been viewed largely as an atmospheric phenomena. However, we show that the global ocean is an important component in determining global surface temperatures. Via an empirical, mathematical methodology, we are able to decompose the non-linear and non-stationary data sets, and reveal buried, internal modes of variability of planetary temperatures over the past 167 years. We find periods of both cooling and warming, both in the ocean and the atmosphere over land, with natural variability ranging from seasonal to annual to inter-annual to multi-year to decadal to multi-decadal to centennial. We find that both the ocean surface and the air over land display non-linear trends depicting initially multi-decadal periods of cooling from the mid to late 19th Century, and then persistent warming throughout the 20th Century and into the 21st Century. Our calculated overall trends of the rates of warming differ significantly from the estimate of the IPCC, with the oceanic rate less than two thirds of that in the atmosphere. It is special note here that while the overall trends of planetary surface trends

indicate persistent and increasing warming (IMFs 10), the 9 higher frequency modes of variability can modulate the overall temperature record from seasonal to centennial time scales. Nonetheless, while the cars on the train may be oscillating with different modulated frequencies (periods), the train is still moving forward.

Empirical relationships between billions of tons of fossil fuel burning and the overall trends of the global surface temperature anomaly time series both in the global ocean, the air above land and the combined global surface temperature anomaly time series emerge from our reduction of the non-stationary, non-linear data. Mathematical relationships between fossil fuel burning and surface temperatures in the oceans and over land are presented. The statistical relationship curves reveal strongly suggest that there is a one-year phase lag between carbon loading and planetary surface temperature rise, and that there is causal correlation in the Granger (1980) sense and that global surface temperatures can be predicted from fossil fuel burning a year earlier. Thus the conclusion is reached that there is attribution and further, if present fossil fuel burning is not curtailed, there will be continued warming of the planet in the future.

Acknowledgements: We thank Dr. Thomas S. Malone (now deceased), member of the U.S. National Academy of Sciences, one of the Founders of the National Center for Atmospheric Research, and a past recipient of the Saint Francis of Assisi Award for the Environment, for having encouraged this study, not long before his passing. The authors also acknowledge Coastal Carolina University and Clemson University for supporting this study. The authors express their appreciation for the arduous efforts that the many unsung heroes who have collected, documented, preserved and protected the precious data archives that scientists need to advance the state of knowledge and understanding of how our planetary climate system works. We also thank Dr. T.Y. Yan and Mr. J. M. Epps for figure contributions, and Dr. P.T. Gayes for helpful discussions.

REFERENCES

- [1] Trenberth, K.E., D.P. Stephaniak, J.M. Caron, 2002. Inter-annual Variations in the Atmospheric heat Budget. *Journal of Geophysical Research*, Vol. 107, No. D8, pp. AAC 4-1 -AAC-4-15. Doi: 10.1029/2000JD000297.
- [2] Trenberth, K.E., 2003. *Handbook of Weather*. T.D. Potter and B.R. Coleman, Eds. Climate and Water. John Wiley and Sons. Hoboken, N.J., pp. 163-173.
- [3] Vogel, J.M. and B. Lazar, 2010. Global Cooling, Science and Myth. *Weatherwise*, Vol. 63, No. 4, pp.24-31. doi: 10.1080/00431672.2010.490166.
- [4] J. I. Antonov, S. Levitus and T. P. Boyer, 2004. Climatological Annual Cycle of Ocean Heat Content, *Geophysical Research Letters*, Vol. 31, No. 4, Article ID: L04304. doi:10.1029/2003GL018851
- [5] T. Kuhlbrodt, A. Griesel, M. Montoya, A. Levermann, M. Hofmann and S. Rahmstorf, 2007. On the Driving Processes of the Atlantic Meridional Overturning Circulation, *Reviews of Geophysics*, Vol. 45, No. 2, Article ID: RG2001. doi:10.1029/2004RG000166
- [6] Levitus, S., J. Antonov, T. Boyer, 2005. Warming of the World's Ocean, 1955-2003. *Geophysical Research Letters*, Vol. 32, No. 2. Article ID: L02604. doi: 10.1029/2004GL021592.
- [7] Sabra, K., B. Cornuelle, W. Kuperman, 2016. Rising Heat Content of the Earth's Oceans. *Physics Today*, p. 32.
- [8] Cheng, L. K. E. Trenberth, J. Fasullo, T. Boyer, J. Abraham, J. Zhu, 2017, Improved Estimates of Ocean Heat Content 1960-2015. *Science Advances*, Volume 3, Number 3.
- [9] Huang, N. E., Z. Shen, S. R. Long, M. C. Wu, E. H. Shih, Q. Zheng, C. C. Tung, and H. H. Liu, 1998: The empirical mode decomposition and the Hilbert spectrum for nonlinear and non-stationary time series analysis. *Proc. Roy. Soc. Lond.*, 454A, 903-993.
- [10] Huang, N. E., Z. Shen, and S. R. Long, 1999: A New View of Nonlinear Water Waves – The Hilbert Spectrum, *Ann. Rev. Fluid Mech.*, 31, 417-457.
- [11] Huang, N. E., M. L. Wu, S. R. Long, S. S. Shen, W. D. Qu, P. Gloersen, and K. L. Fan, 2003: A confidence limit for the Empirical Mode Decomposition and Hilbert Spectral Analysis. *Proc. Roy. Soc. London*, 459A, 2317-2345.
- [12] Wu, Z., and N. E. Huang, 2009: Ensemble Empirical Mode Decomposition: a noise-assisted data analysis method. *Advances in Adaptive Data Analysis*, 1, 1-41.
- [13] Huang, N. E., and Z. Wu., 2008: A review on Hilbert-Huang Transform: the method and its applications on geophysical studies. *Rev. Geophys.*, 46, RG2006, doi:10.1029/2007RG000228.
- [14] Huang, N. E., Z. Wu, S. R. Long, K. C. Arnold, X. Chen, K. Blank, 2009: On instantaneous frequency. *Advances in Adaptive Data Analysis*, 1, 177-229.
- [15] Gabor, D., 1946: Theory of communication, *J. IEE*, 93, 429-457.
- [16] Van der Pol, B., 1946: The fundamental principles of frequency modulation, *Proc. J. IEE*, 93, 153-158.
- [17] Wu, Z., and N. E. Huang, 2004: A study of the characteristics of white noise using the empirical mode decomposition method, *Proc. Roy. Soc. London*, 460A, 1597-1611.
- [18] Flandrin, P., G. Rilling, and P. Goncalves, 2004: Empirical mode decomposition as a filter-bank. *IEEE Signal Proc Lett.*, 11, 112-114.
- [19] James, Glenn; Alchian, Armen Albert; James, Robert C., 1976: *Mathematics dictionary*. Published by Van Nostrand Reinhold Company ISBN 10: 0442240910 ISBN 13: 9780442240912
- [20] Chatfield, C., 1975: *The Analysis of time series: Theory and Practice*. John Wiley & Sons. 263 numbered pages.
- [21] Granger, C.W.J., 1966: The typical shape of an econometric variable. *Econometrica*, 34, 150-161.
- [22] Wu, Z., N. E. Huang, J. M. Wallace, B. V. Smoliak, X. Chen, 2007: On the time-varying trend in global-mean surface temperature. *Climate Dynamics*, Aug. 2011, Vol. 37 Issue 3/4, p.759.

- [23] IPCC Climate Change, 2007: The Physical Science Basis. Summary for Policymakers. Contribution of Working Group I to the Fourth Assessment Report of the Intergovernmental Panel on Climate Change. Geneva, Switzerland: UNEP.
- [24] Boden, T. and R. Andres, 2016. The Carbon Dioxide Information Analysis Center, Oak Ridge National Laboratory, Oak Ridge, Tennessee 37831-6290, USA.
- [25] Marland, G., 2016. The Research Institute for Environment, Energy and Economics, Appalachian State University, Boone, North Carolina 28608-2131, USA.
- [26] Granger, C. W. J. 1980: Testing for causality: A personal viewpoint. *Journal of Economic Dynamics and Control* 2, 329-352.
- [27] Brockwell, P. R. and R. A. Davis, 1991): *Time Series: Theory and Methods* (2nd edn). New York: Springer-Verlag.
- [28] Akaike, H. 1974: A new look at the statistical model identification. *IEEE Trans. Autom. Control* 19, 716-723.